Journal of Materials Chemistry C

Accepted Manuscript

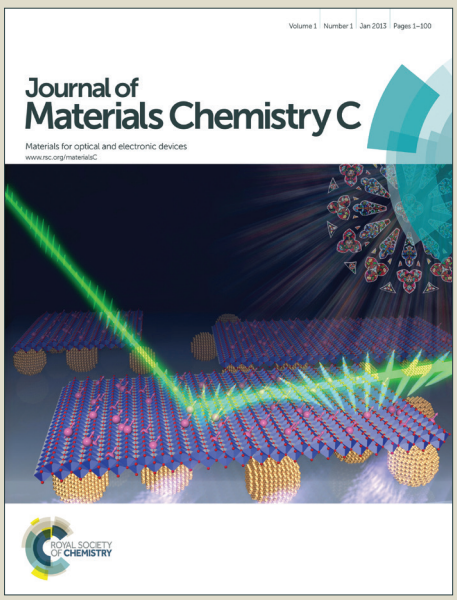

ROYAL SOCIETY OF CHEMISTRY

www.rsc.org/materialsC

Journal Name

ARTICLE

Self-Healing and Phase Behavior of the Self-Healing Liquid Crystalline Elastomer based on Block Copolymer Consisted of Side-Chain Liquid Crystalline Polymer and Hydrogen Bonding Block

Miao Yan[a], Jun Tang[a], He-lou Xie[a]*, Bin Ni[a], Hai-liang Zhang[a]*, Er-qiang Chen[b]

Received 00th January 20xx,
Accepted 00th January 20xx

DOI: 10.1039/x0xx00000x

www.rsc.org/

ABSTRACT: In this paper, we reported a novel multiphase supramolecular liquid crystalline elastomers (LCEs) based on liquid crystalline block copolymer (LCBCP), which consisted of a side-chain liquid crystalline polymer (SCLCP) and a soft segment with hydrogen-bonding. The polymers were "cross-linked" by multiple hydrogen bonds, forming the structure similar to the thermoplastic elastomer (TPE). The SCLCP embedded in soft chain matrix and exhibited physical crosslinking property as well as the enhancement of mechanical properties. At the same time, hydrogen bonds in this new system allowed the self-healing capability of dynamic supramolecular assemblies without any external stimulus, healing agent, plasticizer or solvent. More interestedly, it was found that the introduction of the hydrogen bonding resulted in weakening the ability of the microphase separation of the block copolymer and improving the ordered structure of liquid crystalline phase.

Introduction

Liquid crystalline elastomers (LCEs)[1,2] with the combining properties of the rubber elasticity and the anisotropic liquid crystalline (LC)[3,4] ordering are the promising candidates in multifunctional intelligent materials because of their excellent soft elastic properties, ferroelectric properties, piezoelectric properties, optical nonlinearity, shape memory characteristics and light-induced or thermal induced strain characteristics and so on.[5-13] Generally, LCEs are based on the interpenetrating polymer network (IPN) with low crosslinking density compared to thermoset polymers.[14,15] At the same time, by selecting suitable chemistry moieties of the macromolecular network structure, both the liquid crystalline phase structure and these physical properties can be optimized for specific applications like mechanics, optics, diffusional or electronic transport, etc.[16-24]

Since de Gennes proposed the concept of LCEs in 1975,[25] Finkelmann[26] synthesized the first LCE with the backbone of hydrogenmethyl polysiloxane (PMHS) in 1981. After that, in the past decades several strategies have been developed to prepare the various molecular structures LCEs to realize different properties.[14,16] Generally, the preparation of LCEs is based on well-known principles evaluated for linear liquid crystalline polymers (LCPs). And the polymer includes mesogenic moieties consisted of either rigid rods or discs. The

[a]*Key Laboratory of Special Functional Polymer Materials of Hunan Province, Key Laboratory of Advanced Functional Polymer Materials of Colleges and Universities of Hunan Province and Key Lab of Environment-friendly Chemistry and Application in Ministry of Education, College of Chemistry, Xiangtan University, Xiangtan 411105, Hunan Province, China.*
[b]*Beijing National Laboratory for Molecular Sciences, College of Chemistry and Molecular Engineering, Peking University, Beijing 100871, China.*
** To whom the correspondence should be addressed.*
E-mail: xhl20040731@163.com (HLX)
† Electronic Supplementary Information (ESI) available: See
DOI: 10.1039/x0xx00000x

mesogenic units can be attached either as side chains to the main chain yielding "side chain elastomers" or directly linked together within the polymer backbone yielding "main chain elastomers". An additional variation of the architecture of the network is given by connecting the mesogenic groups via different geometries, e.g., for rods via their long axis ("end-on") or via their short axis ("side-on"). All these different geometries directly affect the LC ordering structure and the polymorphism. As a result, by controlling the molecular structure of LCEs such as mesogenic units, backbones and crosslinking density, diverse characteristics can be introduced into such LCE systems. Also, block copolymers have been used for the formation of supramolecular networks.[26,27] In this case, an artificial muscle with lamellar structure based on a nematic triblock copolymer (RNR) was proposed by Patrick Keller, the material consisted of a repeated series of nematic polymer blocks(N), and conventional rubber blocks (R),[27] in which the crosslinking was present only in the R blocks. This striated structure would be mechanically more robust and the monodomain nematic ordering would be better preserved during the contraction/elongation cycles.

Generally, the internal micro cracks of polymer often weaken mechanical and functional performances in the progress of application. As a result, the idea of self-healing[29-34] property in materials is proposed naturally. Self-healing can be defined as the ability of a material to heal (recover/repair) damages automatically and autonomously. In earlier research, self-healing property is introduced into systems by the release of healing agents.[35-37] Liquid active agents such as monomers, dyes, catalysts and hardeners containing microcapsules,[38-41] hollow fibers,[42,43] or channels are embedded into polymeric systems during its manufacturing stage. In the case of a crack, the reactive agents are poured into the cracks and heal the crack. However, it is necessary that the relieved stress from the crack is a major drawback of this process. Another significant self-healing system consists of polymers with reversible cross-links including covalent bonds[44-47] and noncovalent bonds.[47,48] In the first approach, also referred to "self-repairing", covalent bonds are reshuffled upon application of an external stimulus such as light or heat, cracks in the material will be bridged by newly formed bonds. The introduction of hydrogen bond into polymer is an efficient way to construct self-healing material since the supramolecular reactions are dynamic and can be reconstructed after damage with little external intervention. In the recent researches, a lot of self-healing systems have been put forward, e.g. an elegant dynamic supramolecular approach was developed to obtain a self-healing rubber using multivalent hydrogen bonds.[47-52] By contrast, Guan[53,54] and his coworkers developed a design of multiphase supramolecular thermoplastic elastomers (TPEs) that combine high modulus and toughness with spontaneous healing capability. This new system spontaneously self-heals as a single-component solid material at ambient conditions without any external stimulus, healing agent, plasticizer or solvent, which can make sure the performance of material not to be effected.

In this work, we intend to construct a novel self-healing LCE through the incorporation of multiple hydrogen bonds, which has a similar structure as TPEs. That is, the structure of this kind of self-healing LCE is a typical diblock copolymer consisted of a side-chain liquid crystal polymer (SCLCP) and a soft polymer with hydrogen bonding. The chemical structure of these diblock copolymers (poly ((6-(4-((4-butylphenyl)diazenyl)phenoxy)hexyl methacry-late-*co*-Hexyl methacrylate)-*b*-*N*-acetamidopentyl methacry-late), PM1-*b*-PM(NCP)A) is shown in scheme 1. The BCPs were cross-linked by multiple hydrogen bonds forming the structure of LCEs. The SCLCP chains embedded in soft chain matrix and exhibited physical crosslinking property as well as the enhancement of mechanical properties. At the same time, the reversibility of hydrogen bonds in this new system allowed the self-healing capability of dynamic supramolecular assemblies without any external stimulus. In the meanwhile, we found that the introduction of the hydrogen bonding led to weakening the ability of the microphase separation of the block copolymer and enhancing the ordered structure of LC phase.

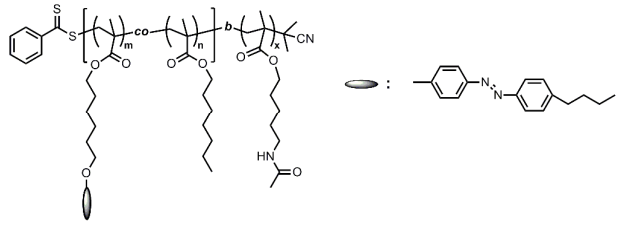

Scheme 1. The chemical structure of LC BCP LCE.

Experimental section

Materials

Phenol (98%, Alfa Aesar), n-butyl phenylamine (98%, Alfa Aesar), 1,6-dibromohexane (98%, Alfa Aesar), methacrylic acid (98%, Alfa Aesar), 5-aminopentanol (97%, Alfa Aesar), 2,2-azobisisobutyronitrile (AIBN, 99%, Aldrich), N,N-dimethylformamide (DMF) (Shanghai Chemical Reagents Co., A.R. grade), and tetrahydrofuran (THF, 99%) were used as received. Chlorobenzene (Aldrich, 99%) was purified by washing with concentrated sulfuric acid to remove residual thiophenes, followed by washing twice with distilled water, once with 5% sodium carbonate solution, and again with water before being dried with anhydrous calcium chloride and then distilled. Acetone (AR, Beijing Chemical) was refluxed over potassium permanganate and distilled before use.

Instruments and measurements

^{1}H NMR spectra were recorded on a Bruker ARX 400 MHz spectrometer with tetramethylsilane (TMS) as the internal standard and $CDCl_3$ or DMSO as the solvent. GPC measurements were carried out at 35 °C on a PL instrument

using DMF as the eluent at a flow rate of 1.0 mL/min. The GPC data were calibrated with PS standards. Thermogravimetric analysis (TGA) was performed on a TA SDT 2960 instrument at a heating rate of 10 °C/min in a nitrogen atmosphere. Differential scanning calorimetry (DSC) experiments were carried out on a TA DSC Q100 calorimeter with a programed heating and cooling procedure in nitrogen. The temperature and heat flow were calibrated with benzoic acid and indium. The samples were encapsulated in hermetically sealed aluminum pans with a typical sample weight of ~5 mg. The cooling and subsequent heating DSC experiments were carried out at a rate of 10 °C/min. LC texture of the polymers was examined under polarized optical microscope (POM, Leica DM-LM-P) coupled with a Mettler-Toledo hot stage (FP82HT). The films with a thickness of ~10 μm were casted from THF solution on glass slides and slowly dried at room temperature. X-ray scattering experiments were performed with a high-flux small angle X-ray scattering (SAXS) instrument (SAXSess, Anton Paar) equipped with Kratky block-collimation system and a Philips PW 3830 sealed-tube X-ray generator (Cu Kα). The scattering pattern was recorded on an imaging plate (IP) with a pixel size of 42.3 × 42.3 μm^2 which is extended to the high-angle region, and therefore the small and wide-angle scattering can be recorded simultaneously. The peak positions were calibrated with silver behenate. After background subtraction, desmearing was performed according to the Lake's method. A temperature control unit (Anton Paar TCS 300) in conjunction with the SAXSess was utilized to study the structures at various temperatures. Finally, the DMA tests were performed with TA instrument of ARES-G2.

Experimental section

The synthetic route of BCPs is outlined in Scheme 2. And the detail information about the synthesis and character of the intermediate and monomers were shown in supplemental information.

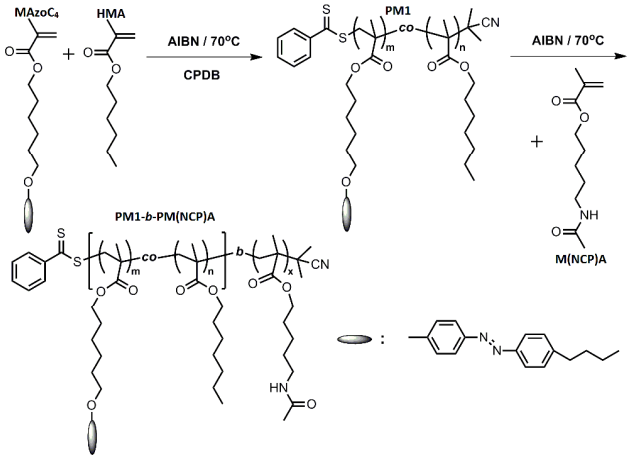

Scheme 2. Synthetic Route of PM1 and the BCPs.

Synthesis of diblock copolymers

As elaborated in supplementary information, a LC monomer (6-(4-((4-butylphenyl)diazenyl)phenoxy)hexyl meth-acrylate, $MAzoC_4$) containing azobenzene and a butyl tail was prepared. With the monomers of $MAzoC_4$ and Hexyl methacrylate (HMA), the Poly (6-(4-((4-butylphenyl)diazenyl) phenoxy)hexyl methacry-late-*co*-Hexyl methacrylate) (PM1) block was synthesized first by using the method of reversible addition-fragmentation chain transfer polymerization (RAFT) as shown in scheme 2. For example, $MAzoC_4$ (1 g, 2.4 mmol), HMA(0.3 g, 1.6 mmol), CPDB (0.01 g, 0.045 mmol), AIBN (0.002 g, 0.012 mmol), and THF (2 mL) were added to a reaction tube. After being degassed with three freeze–thaw cycles, the tube was sealed under vacuum. The polymerization was carried out at 75 ° C for 6 hours. Afterward, the reaction solution was diluted with THF and was then dripped into ether. The solution was passed through an alumina column to remove the catalyst. After a while, fine polymer was obtained after precipitating from a large amount of methanol and was dried in a vacuum oven at room temperature for 24 h. GPC measurements indicated that the sample PM1 possessed the low polydispersity index (PDI) of 1.10 and the number-average molecular weights (Mns) of 1.1 × 10^4 g/mol. The target three diblocks of PM1-*b*-PM(NCP)A (denoted as BCP-1, BCP-2 and BCP-3) were synthesized through RAFT chain extension reaction using the PM1 as the macromolecular chain transfer agent. In typical, M(NCP)A (1 g, 4.7 mmol), PM1 (0.5 g), AIBN (0.002 g, 0.012 mmol), were added to 3 mL chlorobenzene. The polymerization condition and the purification procedure were the same as that used for the synthesis of PM1 block. The apparent Mn and PDI of the resultant diblocks were measured, which were summarized in Table 1. Furthermore, ^{1}H NMR experiments were performed to estimate the composition of PM1 and the BCPs. As mentioned before, PM1 was a copolymer of $MAzoC_4$ and HMA, and the two monomers involved were quite different in chemical structure. According to the the ^{1}H NMR spectra of PM1 and the BCPs as shown in S-Figure 2 of the supplemental information, the mole fraction of $MAzoC_4$ can be calculated according to eq. 1 presented as below.

$$f_{\mathrm{PMAzoC4}} = \frac{\mathbf{a}}{\mathbf{a}+1} \;; \qquad \mathbf{a} = \frac{\frac{34}{4} \times I_{\mathrm{i+j+k+l}}}{I_{\mathrm{total}} - \frac{34}{4} \times I_{\mathrm{i+j+k+l}}} \times \frac{18}{34} \qquad \textbf{Eq. 1.}$$

In the equation, f_{PMAzoC4} means the mole fraction of $PMAzoC_4$ in PM1; the value of 34 and 18 are the sum of proton numbers in $MAzoC_4$ and HMA respectively; the value of 4 is the proton numbers of the azobenzene groups; $I_{\mathrm{i+j+k+l}}$ and I_{total} are the integral intensities of the signals at 7.7 to 7.9 and 0 to 8.0 ppm, respectively. When it came to the mole fraction calculation of each block for BCPs, the equation seems to be more complicated since the composition of copolymer had to be taken into account at the same time. As a result, the

equation for the calculation of mole fraction of PM1 block (f PM1) in BCPs can be modified as follow:

$$f_{Sx} = \frac{a'}{a'+1} \qquad f_{PM(NCP)A} = \frac{1}{a'+1}$$

Eq. 2.

$$a' = \frac{\frac{34 f_{PMAzoC4} + 18 f_{PHMA}}{4 f_{PMAzoC4}} \times I'_{i+j+k+l}}{I'_{total} - \frac{34 f_{PMAzoC4} + 18 f_{PHMA}}{4 f_{PMAzoC4}} \times I'_{i+j+k+l}} \times \frac{19}{34 f_{PMAzoC4} + 18 f_{PHMA}}$$

In eq. 2, the value of 19 are the sum of proton numbers in M(NCP)A; $I'_{i+j+k+l}$ and I'_{total} are the integral intensities of the signals at 7.7 to 7.9 and 0 to 8.0 ppm for BCPs, respectively. Consequently, we estimate the mole fraction values according to eq. 1 and eq. 2 and the corresponding weight fraction values are calculated. The resulted values of f PM1 ranges from 28.4 % to 52.1 % for the three BCPs synthesized (see table 1).

Table 1. Molecular Characteristics Results of $PMAzoC_4$, PM1 and the BCPs.

Sample	Mn ($\times 10^4$)[a]	PDI[a]	$f_{PM(NCP)A}$ (%)[b]	ΔH (J/g)[c]
$PMAzoC_4$	1.5	1.11	/	/
PM1	1.1	1.10	/	12.42
BCP-1	2.0	1.14	47.9	7.79
BCP-2	3.0	1.17	59.5	4.36
BCP-3	3.8	1.10	71.6	3.68

[a] Detected from PL GPC results, linear PS as standards.
[b] Determined from 1H NMR results using eq. 1 and eq. 2.
[c] ΔH are the enthalpies of the phase transition measured from DSC cooling scan.

Results and Discussion

Dynamic modulus and self-healing property of the BCPs

The resulting BCPs exhibited elasticity similar to rubber at room temperature as expected. As for rubber, the viscoelastic property of polymeric materials is one of the most important properties, and dynamic mechanical analysis (DMA) is an effective technique to study the viscoelastic behavior of polymers. Herein, DMA was carried out to identify their dynamic moduli. A sinusoidal stress is applied and the strain in the material is measured, allowing one to determine the complex modulus. The temperature of the sample or the frequency of the stress is often varied, leading to variations in the complex modulus. The testing results for the BCPs at room temperature are presented in Figure 1, where G' and G'' denotes shear storage and loss moduli respectively, and tanδ is defined as the ratio between G'' and G' indicating the viscoelastic properties. For BCP-1 , the shear storage values (G') were located between 5×10^5 dym/cm^2 and 6×10^5 dym/cm^2 when the strain was below 20 %, while the loss moduli values (G'') were around 3×10^5 dym/cm^2, and the corresponding tanδ was about 0.5, indicating the modest viscoelastic property. In contrast, for BCP-2 and BCP-3 with a higher weight fraction of PM(NCP)A block, the situation presented a little different. The loss moduli values (G'') slightly increased in an order from BCP-2 to BCP-3 while shear storage values (G') remained almost the same respectively. As a result, the corresponding tanδ values increased to 0.61 and 0.73 for each BCP. All these recorded results indicated the three BCP samples had the viscoelastic property of the elastomers. In particular, the dynamic modulus were recorded at around 25 °C, meaning that the BCPs could show rubberlike features at room temperature, which further was helpful to study the self-healing property of the BCPs at relatively low temperatures.

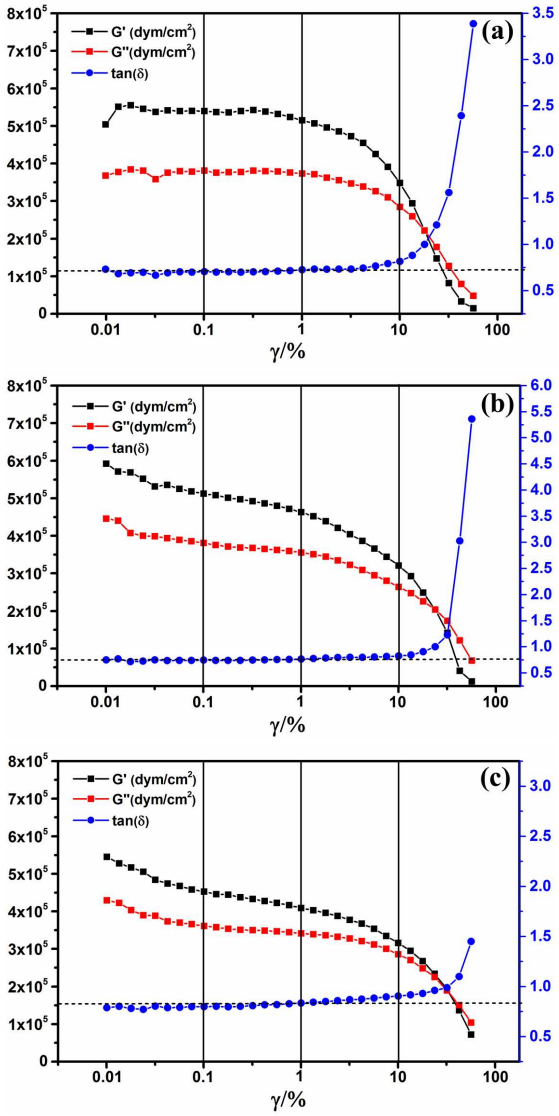

Figure 1. DMA results of the BCP-1 (a), BCP-2 (b) and BCP-3 (c) at room temperature.

The introducing of multiple hydrogen bonds into the BCP system would certainly influence the performance of the material. The dynamic reversibility of hydrogen bonds provided necessary structural basis for the self-healing property in particular. As a result, the self-healing experiment under relatively low temperatures for the BCPs was performed and discussed logically. As described in Figure 2, after cutting a sample into two completely separate pieces at room temperature with a razor blade and gently bringing the cut pieces back into contact, the two faces spontaneously self-healed over time under ambient conditions without any treatment.

It could be obviously observed that the two cut pieces were connected as a single-piece with a healing mark after 30 min. And the mark became indistinct when the sample was treated at 50 °C for another 30 min (Figure 2(c)), indicating a well healing generated on the cut surfaces by the reconnecting of multi-hydrogen bonds. The results different seal-healing time(for 5, 10 and 20 min) at 50 ^{o}C were provided for clear process of self-healing in S-Figure 3 of supplementary information. Furthermore, a supplementary experiment was carried out to investigate the self-healing property of BCP-3 when multiple damages happened as shown in Figure 2. The BCP-3 sample was put into liquid nitrogen until multiple brittle fractures happened but the sample still held as one whole piece (Figure 2(d)). Then the sample was carefully preserved at 50 °C for 3 hours (Figure 2(e)). The result proved that it required longer time for the sample to self-heal than that of the previous experiment. At the same time, some defect remained on the edge of the sample due to the loose contact of the surfaces, where hydrogen bonds could not reconnect well. As for the BCP-1, although the same test was employed, the result seemed unsatisfactory compared with BCP-2 and BCP-3, which was probably because that the fraction of PM(NCP)A containing hydrogen bonding was not that sufficient.

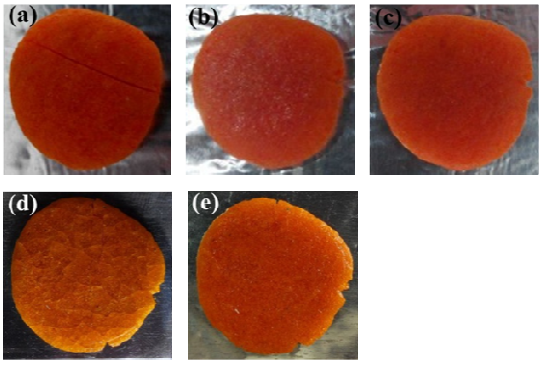

Figure 2. Self-healing test of BCP-3, (a) Cut at room temperature, (b) warming at 50 °C for 30 min, (c) warming at 50 °C for 60 min; (d) brittle fracture in liquid nitrogen, (d) warming at 50 °C for 3 hours.

In order to understand the self-healing mechanism in our BCP system, the FTIR experiment was carried out to investigate the reversible interaction of hydrogen bonding by varying temperatures. A dilute solution (chloroform) of each sample was cast on KBr pallet and allowed to completely dry before measurement. The results showed that all the three BCP samples exhibited the similar infrared spectrum. Here, the FTIR spectrum curves of BCP-2 under different temperature values were presented as an example as shown in Figure 3. In this case, the C=O stretching signals of amide (1652 cm^{-1}) shifted toward higher wave numbers (1680 cm^{-1}), whereas the N-H bending signals (1558 cm^{-1}) shifted toward lower wave numbers (1540 cm^{-1}) from 20 °C to 200 °C. Both these shifts indicated the dissociation of multi-hydrogen bonds between N-H and C=O species when the temperature increased. When the sample was subsequently cooled to room temperature, its FTIR spectrum was almost identical to that before heating. The FTIR results proved the existence of hydrogen bonding at certain temperatures below 120 °C, which explained the self-healing mechanism during the cut/reconnected process in return. On the other hand, the dissociation of hydrogen bonds at above 100 °C would lead to some property changes like the microphase separation structure and the LC property, which would be discussed later in detail.

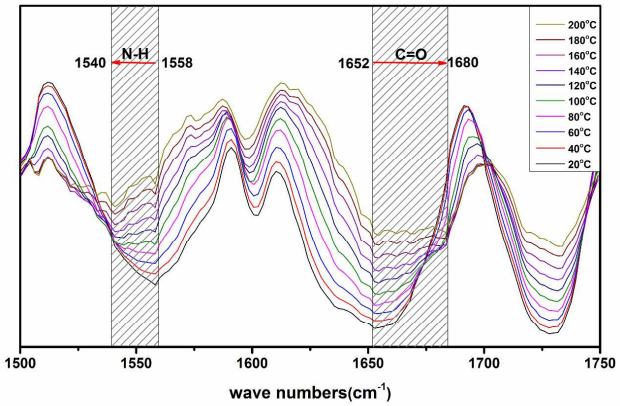

Figure 3. FTIR spectra traces of BCP-3 at various temperatures.

The experimental results above indicated that the BCPs had the viscoelastic property similar to TPEs. At the same time, the BCP samples showed a well self-healing property with the introducing of hydrogen bonding. Combining the chemical structure of BCPs, we proposed a possible morphology of the BCPs in aggregation during the self-healing process, as presented in scheme 3, where microphase separation happened and the SCLCP chains embedded in soft chain matrix. After the polymer material was cut into two pieces and bringing them back into contact closely, multiple hydrogen bonds at the cut faces would reconnect and further lead to the self-healing of the sample under ambient conditions.

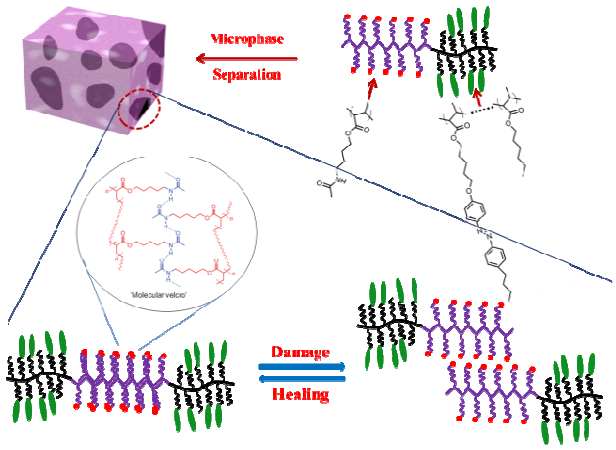

Scheme 3. The aggregation morphology and the self-healing process of the BCPs.

Microphase Separation of PM1-*b*-PM(NCP)A

It is very important to study the microphase behavior and LC behavior for understanding the relationship between the structure and performance during the self-healing progress. Thus, we further investigated the microphase separation structure of the self-healing elastomer. Generally, introduction of LC block into BCP would result in the increase of the segment–segment interaction parameter (χ) and the microphase separation became stronger than that of coil–coil BCP. Especially for rod–coil BCPs, the microphase separation can occur even when their MWs are very low. Among various morphologies of BCPs, lamellar phase appears over a wide range of composition. Herein, SAXS experiments were carried out for the three BCP samples of PM1-*b*-PM(NCP)A, as presented in Figure 4. Before the SAXS experiment, each solution cast sample was subjected to 12 h of annealing at 90 °C followed by cooling to room temperature at the rate of 10 °C/min. The fitted curves by Lorentz were also presented which were smoother than the original ones as presented in Figure 4.

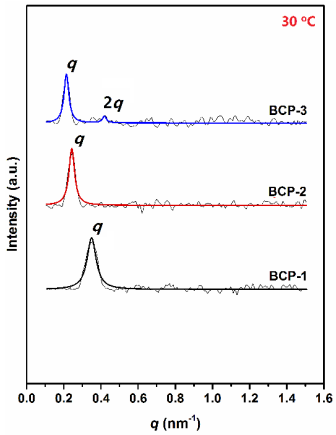

Figure 4. SAXS profiles for the BCPs at 30 °C.

For BCP-3, the lamellar morphology was evidenced by the scattering peaks with a *q*-ratio of 1:2 at around 30 °C, and its layer periods was 27.3 nm. However, only one scattering peak was observed in the SAXS pattern of BCP-1 and BCP-2, which had a lower $V_{PM(NCP)A}$ compared with the other two BCP samples, which could not determine the morphology. As a matter of fact, above 100 °C the second scattering peak of the sample BCP-2 could also successfully develop, and the *q*-ratio also is 1:2, indicating the formation of lamellar structure.

In the meanwhile, variable-temperature SAXS experiments were carried out to investigate the relationship between the phase morphology and temperature. The typical scattering profiles of BCP-3 recorded at different temperatures are shown in Figure 5. And the other two scattering profiles of BCP-1 and BCP-2 are presented in S-Figure 4 and S-Figure 5. The scattering peaks for BCP-1 remained almost the same with increased temperature. While as for BCP-2 and BCP-3, the results seemed to be quite interesting, that was, only one scattering peak was identified for each BCP sample at below 80 °C, and a second peak appeared when the temperature continued increased to 100 °C, indicating the formation of a lamellar structure in BCP-2 and BCP-3. In general, the development of lamellar nanostructure became more obvious with the increasing $V_{PM(NCP)A}$ value from the sample BCP-1 to the sample BCP-3. Obviously, the evolution of the morphology well agrees with the formation of hydrogen bonding in variable-temperature FTIR experiment as shown Figure. 3, which indicates that the hydrogen-bond interaction is unfavourable to the form a higher ordered nanostructure by microphase separation. At same time, this effect seems to be weakened as the interactions became weaker when the temperature increased.

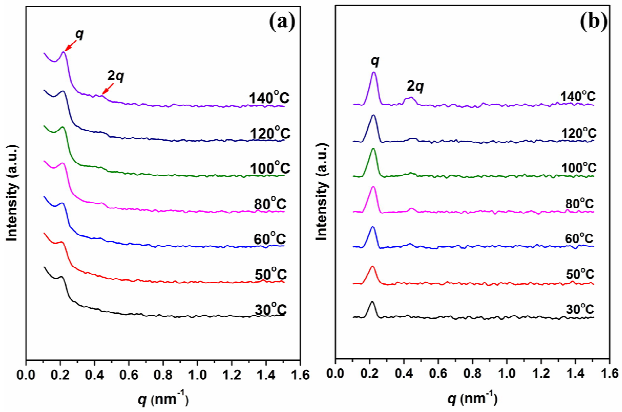

Figure 5. SAXS profiles of BCP-3 (a) and curves fitted from (a) by Lorentz transformation function (b) at different temperatures.

In the previous part, we discussed the dependence of hydrogen bonding interaction on temperature by FTIR and it proved that this interaction was weakened as the temperature increased. Although microphase separation occurred in the BCPs, there might still exist the association of hydrogen bonds between PM1 and PM(NCP)A blocks below 100 °C, which was

helpful to prospective possibility on the self-healing property. And the entanglement of macromolecular chains was also enhanced by the interaction of hydrogen bonding, leading to the less distinct interface between the two blocks. Thus, this interaction went against the microphase seperation. When the temperature further increased, the dissociation of multi-hydrogen bonds became possible and a distinct lamellar nanostructure by microphase separation was developed.

Phase behavior and LC properties of PM1 and the BCPs

Phase behavior and LC properties of PM1 and the BCPs. As mentioned in the experimental section, PM1 was a copolymer of $MAzoC_4$ and HMA. In order to further understand LC property of the designed random copolymer and its corresponding BCPs, a homopolymer sample ($PMAzoC_4$) was prepared for comparison with the Mn of 1.5×10^4 and PDI of 1.10. Meanwhile, the question about how the introducing of PHMA affected the copolymer system both structurally and functionally could be also investigated by comparison.

Phase transition behaviors of the homopolymer ($PMAzoC_4$), random copolymer (PM1) as well as three BCP samples were investigated using DSC. First of all, we'd like to discuss the different phase behaviors between $PMAzoC_4$ and random copolymer PM1 containing PHMA. Figure 6 depicts a set of DSC traces recorded upon the first cooling and the second heating process of the samples at a rate of 10° C/min.

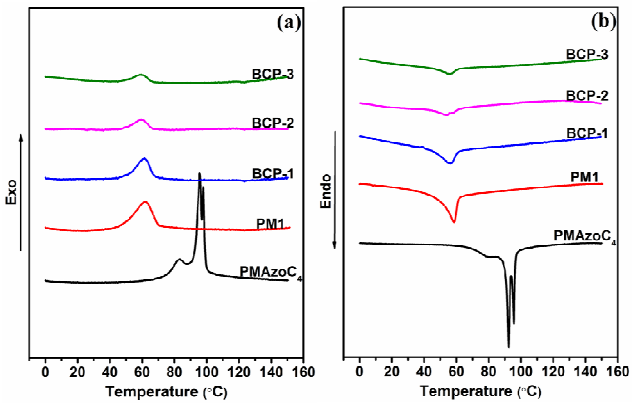

Figure 6. DSC traces of the $PMAzoC_4$, macro-chain transfer agent (PM1) and the BCPs recorded during the first cooling (a) and the second heating (b) at a rate of 10° C/min.

It was obvious to find that the $PMAzoC_4$ had a phase transition at around 85 °C, corresponding to a high order smectic phase (SmX) similar to the results of Iyoda's reseach.[55] Two other transitions could also be observed at the same time upon heating which attribute to the melt of smectic A (SmA) phase and the entrance of isotropic state from nematic phase, respectively. While on the other hand, the DSC traces of PM1 indicated quite different phase behaviors from the $PMAzoC_4$. Only one thermal transition peak was observed for PM1 at around 60 °C, which indicated that the PHMA part in copolymer PM1 played a very important role in phase transition properties. The introduction of the PHMA in this copolymer may suppress the development of LC high order structure, thus, we speculated the two transitions could be the transition from smectic to nematic state and a transition from nematic to isotropic state.

The block copolymer samples exhibited one broad phase transition peak at around 60 °C similar to the result of PM1. The enthalpies (ΔH) of PM1 and the BCPs were calculated during the transition process. As presented in Table 1, the ΔH values slightly decreased with the increase of weight fraction of PM(NCP)A in block copolymers, and enthalpy for each BCPs was smaller than that of PM1. We considered that the PM(NCP)A block located near to the phase boundary was in a disordered state, which might be caused by an irregular structure at the interface. At the same time, the microphase separation on the interface of PM1 and PM(NCP)A also had an effect on ΔH. The interplay of these two factors in the BCPs led to the slight changes in ΔH values. It's worth mentioning that the network cross-linked by hydrogen bonds in BCPs may transfer some energy during phase transition to the whole polymer system, which was hardly detected by the instrument.

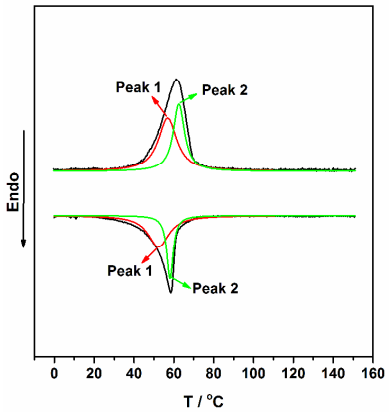

Figure 7. Fitted DSC curves of the PM1 by Lorentz transformation function.

LC properties of $PMAzoC_4$, copolymer PM1 and the BCPs were confirmed by POM experiments. As shown in Figure 8 (a)–(e). Although the birefringence of LC phase of each sample was obvious, typical LC textures were hard to be identified under POM in general. For PM1, it might be due to that the PHMA part restrained the ordered structure of the mesogens. And as for the BCPs, this result could be explained by the fact that the development of large LC domain was suppressed by the formation of microphase-separated structure. Interestingly, for the block copolymer BCP-1, the birefringence of LC phase was more distinct than PM1 as well as that of the two other BCP samples. We speculated this was probably because in BCP-1 the weight fraction of PM(NCP)A block was relatively small, and the microphase-separated structure was

not so obvious that the hydrogen bonds promoted the mesogens to form a more ordered structure.

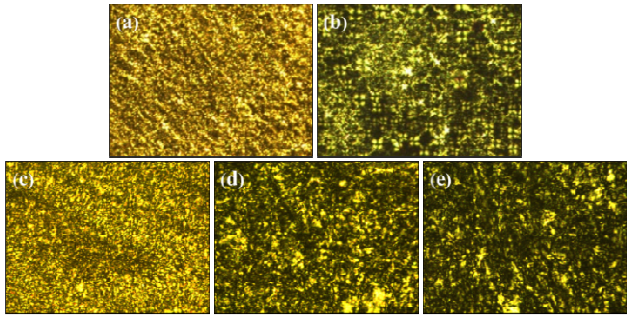

Figure 8. POM images of $PMAzoC_4$ (a), PM1 (b), BCP-1 (c), BCP-2 (d), and BCP-3 (e) (500× magnification) obtained at room temperature.

Furthermore, the LC phase structure could be precisely detected by X-ray diffraction (XRD). All samples were heated above their isotropic temperature (Ti) followed by slow cooling to room temperature at 2 °C/min. Figure 9 describes the XRD patterns of homopolymer ($PMAzoC_4$), PM1 and three PM1-*b*-PM(NCP)As (BCPs) at room temperature. Some clear diffraction peaks were observed in low-angle regions, which corresponded to the existence of ordered structures on nanometer length scale. $PMAzoC_4$ exhibited two diffraction peaks (q and $2q$) in low-angle regions located at 2.2 nm^{-1} and 4.4 nm^{-1}, indicating the formation of lamellar structure. In contrast, the patterns of PM1 and BCPs were similar to that of $PMAzoC_4$, the intensity of the diffraction peaks remarkably decreased with the introducing of PHMA. However, the sample BCP-1 showed a diffraction enhancement compared with PM1, which was consistent with the POM results. In addition to XRD experiments at room temperature, diffraction patterns were also recorded by varying temperature.

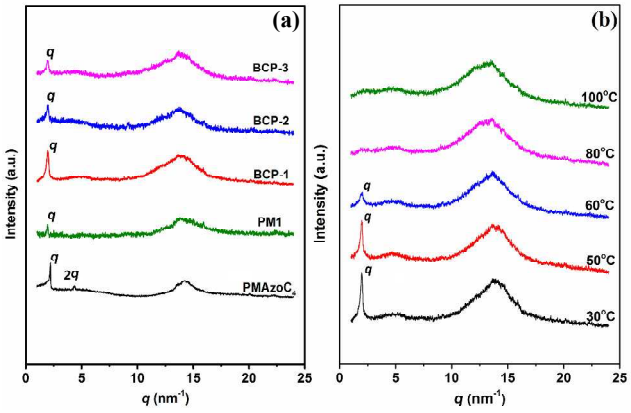

Figure 9. (a) X-ray diffraction patterns for $PMAzoC_4$, PM1 and BCPs at room temperature and (b) for BCP-1 at various temperatures.

As presented in Figure 9(b) of the sample BCP-1, it's obvious that the diffraction peak intensity decreased with the elevation of temperature until each peak vanished above 80 °C, which was in good agreement with the isotropic temperature value of DSC for each polymer sample. And the data of the other samples was shown in S-Figure 6.

In order to further investigate the LC structure, 2D-WAXD experiments were carried out for the oriented fibre samples of PM1 and the BCPs. The diffraction images of each sample were recorded and analyzed respectively before and after annealing at around 70 °C corresponding to their isotropic temperature. In Figure 10, typical diffraction textures of the polymer samples are presented (Figure 10(a)-(d)). (The completely whole graphs were shown in S-Figure 7). For PM1, the diffraction arcs were quite obscure. While for the BCPs, the diffraction arcs became much more distinct comparing to that of PM1, which was corresponded to the results of XRD as mentioned above. In the meanwhile, SmA phase of the polymers could be also identified according to the 2D-WAXD results, which was in agreement with the DSC results. At the same time, the 1D-WAXD curves transferred from 2D-WAXD data is shown in Figure 10(e), and the transformation of the intensity well agreed with the X-ray diffraction patterns as shown in the Figure 9(a).

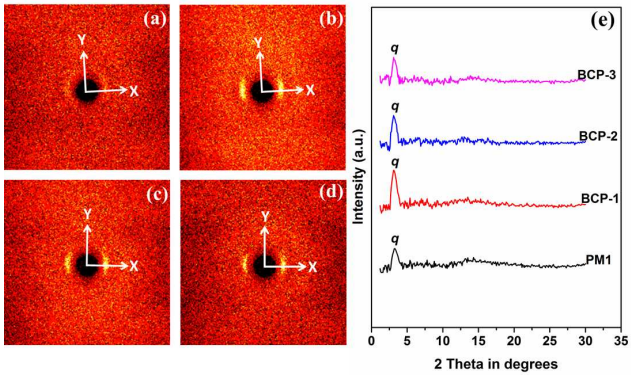

Figure 10. Enlarged 2D-WAXD patterns of PM1 (a), BCP-1 (b), BCP-2 (c), BCP-3 (d) and 1D-WAXD curves (e) transferred from 2D-WAXD data at room temperature. (Y as the shear direction with X-ray verticle to the XY plane)

It is well known that the phase morphology of BCP containing LC block can have an important influence on the LC transitions due to the presence of BCP interface and any geometrical or confinement effects that the interface introduced. Ober et al.[56] have found that in azobenzene-functionalized BCPs, the effect of the BCP morphology on LC phase could be considered into two aspects, that was, the cylindrical morphology could stabilize the smectic phase but the lamellar morphology gave destabilization of the LC phase. The reason may be associated with the compatibility of the blocks and the relative flexibility or chemical structure of the LC polymer backbone. In our case, the stability of LC phase for BCPs seemed to have increased according to X-ray experiments by varying temperature. This result was probably due to the hydrogen-bond interaction within the BCP system.

Conclusions

In this work, we have synthesized a serious of SCLCP BCPs, i.e., PM1-*b*-PM(NCP)A via RAFT with the structure of TPE and multiple hydrogen bonds. Especially, the monomer HMA was introduced into PM1 to decrease the glass transition temperatures of the BCPs. Viscoelastic properties of BCPs were investigated by DMA tests, indicating the BCPs could show rubberlike features at room temperature. Self-healing property of BCP-3 was investigated as an example and the results revealed that after cutting a sample into two completely separate pieces at room temperature with a razor blade and gently bringing the cut pieces back into contact, the two faces spontaneously self-healed over time under ambient conditions without any treatment. When further investigating the self-healing mechanism and the aggregation morphology of the BCP elastomers by FTIR and SAXS, we found that the hydrogen bonding played a very important role in microphase separation and the morphology of the BCPs. The disassociation of hydrogen bonding at high temperature led to a more distinct interface between the two blocks and a formation of a more ordered microphase separated structure of the BCPs. DSC, POM and XRD experimental results indicated an enhancement in the LC order of the BCPs with the incorporation of multiple hydrogen bonds.

Acknowledgements

This research is financially supported by the National Nature Science Foundation of China (21374092 and 21104062), the project of Hunan Provincial Education Department (YB2013B032), Innovation Platform Open Foundation of University of Hunan Province (14K093) and Beijing National Laboratory for Molecular Sciences (BNLMS).

Notes and references

1. R. Zentel, *Adv. Mater.,* **1989**, *1*, 321.
2. H. Yang, Z. L. Wu and P. Keller In *Handbook of Liquid Crystals*; Wiley-VCH Verlag GmbH & Co. KGaA: 2014.
3. A. Ciferri *Polymer liquid crystals*; Elsevier, 2012.
4. A. M. Donald, A. H. Windle and S. Hanna *Liquid crystalline polymers*; Cambridge University Press, 2006.
5. S. Baljeet, *J. Phys. D.,* **2007**, *40*, 584.
6. H. R. Brand, H. Finkelmann, D. Demus, J. Goodby, G. W. Gray, H. W. Spiess and V. Vill In *Handbook of Liquid Crystals Set*; Wiley-VCH Verlag GmbH: 2008, p 277.
7. H. R. Brand, H. Pleiner and P. Martinoty, *Soft Matter,* **2006**, *2*, 182.
8. M. Brehmer, R. Zentel, F. Gießbtelmann, R. Germer and P. Zugenmaier, *Liq. Cryst.,* **1996**, *21*, 589.
9. T. Ikeda, J.-i. Mamiya and Y. Yu, . *Chem. Int. Ed.,* **2007**, *46*, 506.
10. W. Lehmann, H. Skupin, C. Tolksdorf, E. Gebhard, R. Zentel, P. Krüger, M. Lösche and F. Kremer, *Nature,* **2001**, *410*, 447.
11. I. A. Rousseau and P. T. Mather, *J. Am. Chem. Soc.,* **2003**, *125*, 15300.
12. R. Stannarius, R. Köhler, U. Dietrich, M. Lösche, C. Tolksdorf and R. Zentel, *Phys. Rev. E,* **2002**, *65*, 041707.
13. H. Yang, A. Buguin, J.-M. Taulemesse, K. Kaneko, S. Méry, A. Bergeret and P. Keller, *J. Am. Chem. Soc.,* **2009**, *131*, 15000.
14. D. L. Thomsen, P. Keller, J. Naciri, R. Pink, H. Jeon, D. Shenoy and B. R. Ratna, *Macromolecules,* **2001**, *34*, 5868.
15. K. A. Burke and P. T. Mather, *J. Mater. Chem.,* **2010**, *20*, 3449.
16. P. Xie and R. Zhang, *J. Mater. Chem.,* **2005**, *15*, 2529.
17. M. Chambers, H. Finkelmann, M. Remskar, A. Sanchez-Ferrer, B. Zalar and S. Zumer, *J. Mater. Chem.,* **2009**, *19*, 1524.
18. Y. Jiang, D. Xu, X. Li, C. Lin, W. Li, Q. An, C.-a. Tao, H. Tang and G. Li, *J. Mater. Chem.,* **2012**, *22*, 11943.
19. G.-H. Wen, B. Zhang, H.-L. Xie, X. Liu, G.-Q. Zhong, H.-L. Zhang and E.-Q. Chen, *Macromolecules,* **2013**, *46*, 5249.
20. H.-L. Xie, S.-J. Wang, G.-Q. Zhong, Y.-X. Liu, H.-L. Zhang and E.-Q. Chen, *Macromolecules,* **2011**, *44*, 7600.
21. H.-L. Xie, C.-K. Jie, Z.-Q. Yu, X.-B. Liu, H.-L. Zhang, Z. Shen, E.-Q. Chen and Q.-F. Zhou, *J. Am. Chem. Soc.,* **2010**, *132*, 8071.
22. D. We, B. i Annie, A. Pierre-antoine, P. Keller, X. G Wang and M.H Li, *Chinese Journal of Polymer Science* , 2012, **30**, 258.
23. Q. Bi-wei, C. Feng, S. Yong-gang, L. Yu and Q Zhen., *Chinese Journal of Polymer Science*, 2015, **33**, 95.
24. X B Liu., Y. F Zhu, . H Fan and E. Q Chen, *Chinese Journal of Polymer Science*, 2013, **31**, 946.
25. P.de Gennes, *CR Acad. Sci. B 1975, 281, 101-103.*
26. H.Finkelmann; G.Rehage,. *Die Makro. Chem., Rapid. Comm. 1982, 3 (12),859-864.*
27. H. Xing, J. Li, J. Guo and J. Wei, *J. Mater. Chem. C,* **2015**, *3*, 4424.
28. P.-G. de Gennes and J. Prost, *Oxford University Press, USA,* **1995**, 0.20.
29. J. Schätzle and H. Finkelmann, *Mol. Cryst. Liq. Cryst.,* **1987**, *142*, 85.
30. M. H. Li, P. Keller, J. Yang and P. A. Albouy, *Adv. Mater.,* **2004**, *16*, 1922.
31. S. V. Ahir, A. R. Tajbakhsh and E. M. Terentjev, *Adv. Funct. Mater.,* **2006**, *16*, 556.
32. H. Jonkers In *Self Healing Materials*; S. van der Zwaag, Ed.; Springer Netherlands: 2007; Vol. 100, p 195.
33. N. K. Guimard, K. K. Oehlenschlaeger, J. Zhou, S. Hilf, F. G. Schmidt and C. Barner-Kowollik, *Macromol. Chem. Phys.,* **2012**, *213*, 131.
34. X. Xing, L. Li, T. Wang, Y. Ding, G. Liu and G. Zhang, *J. Mater. Chem. A,* **2014**, *2*, 11049.
35. H. B. Yue, J. P. Fernandez-Blazquez, D. F. Beneito and J. J. Vilatela, *J. Mater. Chem. A,* **2014**, *2*, 3881.
36. D. Y. Zhu, B. Wetzel, A. Noll, M. Z. Rong and M. Q. Zhang, *J. Mater. Chem. A,* **2013**, *1*, 7191.
37. Y. Lin and G. Li, *J. Mater. Chem. B,* **2014**, *2*, 6878.
38. S. H. Cho, H. M. Andersson, S. R. White, N. R. Sottos and P. V. Braun, *Adv. Mater.,* **2006**, *18*, 997.
39. K. S. Toohey, N. R. Sottos, J. A. Lewis, J. S. Moore and S. R. White, *Nat Mater,* **2007**, *6*, 581.
40. H. Wei, Y. Wang, J. Guo, N. Z. Shen, D. Jiang, X. Zhang, X. Yan, J. Zhu, Q. Wang, L. Shao, H. Lin, S. Wei and Z. Guo, *J. Mater. Chem. A,* **2015**, *3*, 469.
41. Y. Zhao, W. Zhang, L.-p. Liao, S.-j. Wang and W.-j. Li, *Appl. Surf. Sci.,* **2012**, *258*, 1915.
42. M. Huang, H. Zhang and J. Yang, *Corrosion Science,* **2012**, *65*, 561.
43. H. Jin, C. L. Mangun, D. S. Stradley, J. S. Moore, N. R. Sottos and S. R. White, *Polymer,* **2012**, *53*, 581.
44. Y.-K. Song, Y.-H. Jo, Y.-J. Lim, S.-Y. Cho, H.-C. Yu, B.-C. Ryu, S.-I. Lee and C.-M. Chung, *ACS Appl. Mat. Interfaces.,* **2013**, *5*, 1378.
45. J. W. C. Pang and I. P. Bond, *Compos. Sci. Technol.,* **2005**, *65*, 1791.

46. M. Wu, B. Johannesson and M. Geiker, *Constr. Build. Mater.,* **2012**, *28*, 571.
47. Y. Amamoto, J. Kamada, H. Otsuka, A. Takahara and K. Matyjaszewski, *Angew. Chem. Int. Ed.,* **2011***,50,*1660.
48. K. Imato, M. Nishihara, T. Kanehara, Y. Amamoto, A. Takahara and H. Otsuka, *Angew. Chem. Int. Ed.,* **2012**, *51*, 1138.
49. N. Bai, K. Saito and G. P. Simon, *Polym. Chem.,* **2013**, *4*, 724.
50. P. Cordier, F. Tournilhac, C. Soulie-Ziakovic and L. Leibler, *Nature,* **2008**, *451*, 977.
51. M. Zhang, D. Xu, X. Yan, J. Chen, S. Dong, B. Zheng and F. Huang, *Angew. Chem. Int. Ed*., **2012**, 51, 7011.
52. J. Cui and A. d. Campo, *Chem. Commun.,* **2012**, *48*, 9302.
53. Y. Chen, A. M. Kushner, G. A. Williams and Z. Guan, *Nat. Chem.,* **2012**, *4*, 467.
54. J. Hentschel, A. M. Kushner, J. Ziller and Z. Guan, *Angew. Chem. Int. Ed.,* **2012***, 51,* 10561.
55. Y. Tian, K. Watanabe, X. Kong, J. Abe and T. Iyoda, *Macromolecules,* **2002**, *35*, 3739.
56. G. Mao, J. Wang, S. R. Clingman, C. K. Ober, J. T. Chen and E. L. Thomas, *Macromolecules,* **1997**, *30*, 2556.

Graphic Abstract

Self-Healing and Phase Behavior of the Self-Healing Liquid Crystalline Elastomer based on Block Copolymer Consisted of Side-Chain Liquid Crystalline Polymer and Hydrogen Bonding Block

Yan Miao[a], Jun Tang[a], He-lou Xie[a]*, Bin Ni[a], Hai-liang Zhang[a]*, Er-qiang Chen[b]

[a]*Key Laboratory of Special Functional Polymer Materials of Hunan Province, Key Laboratory of Advanced Functional Polymer Materials of Colleges and Universities of Hunan Province and Key Lab of Environment-friendly Chemistry and Application in Ministry of Education, College of Chemistry, Xiangtan University, Xiangtan 411105, Hunan Province, China*

[b]*Beijing National Laboratory for Molecular Sciences, College of Chemistry and Molecular Engineering, Peking University, Beijing 100871, China*

* *To whom the correspondence should be addressed.*

E-mail: xhl20040731@163.com (HLX)

Self-healing liquid crystalline elastomers were fabricated using a side-chain liquid crystal polymer and a soft polymer with hydrogen-bonding. Hydrogen-bonding in this system not only was the origin of self-healing effect and played an important role in the microphase seperation and liquid crystalline phase behavior.